RSC Advances

ROYAL SOCIETY OF CHEMISTRY

www.rsc.org/advances

High pressure superconducting phase of BI_3: An *ab initio* study

Defang Duan, Xiaoli Huang, Changbo Chen, Fubo Tian, Kuo Bao, Da Li, Yunxian Liu, Hongyu Yu, Bingbing Liu and Tian Cui*

State Key Laboratory of Superhard Materials, College of Physics, Jilin University, Changchun 130012, People's Republic of China

*Corresponding Author: E-mail: cuitian@jlu.edu.cn

Abstract

Using the *ab initio* evolutionary algorithm for crystal structure prediction, we successfully obtained the high pressure crystal structure of BI_3 with $P2_1/c$ space group, which characterized as B_2I_6 dimer analogous diborane molecule. This structure has been supported by the excellent agreement between theoretical and experimental equation of states, X-ray diffraction data, and the positive pressure dependence of T_c. Moreover, the $P2_1/c$ structure is both dynamically and mechanically stable through phonon and elastic constants calculation. Further analysis reveals a superconducting mechanism that iodine atoms vibrations dominate the superconductivity of BI_3. Additionally, the positive pressure dependence T_c is mainly attributed to the increase of EPC parameter λ, the logarithmic average phonon frequency ω_{log}, and electronic density of states at the Fermi level $N(\varepsilon_f)$.

Key words: *ab initio* calculations; high pressure; dimerization; superconductivity

Introduction

Molecular crystals have drawn considerable attention for many years and have been studied extensively to understand the relationship between structure and properties.[1, 2] The weak intermolecular interactions, such as van der Waals force, electrostatic force and hydrogen bond, play fundamental roles in defining crystal and electronic structures of molecular crystals. High pressure can significantly reduce the distance between molecules and change the strength of intermolecular interactions, give rise to a variety of novel phenomenon in molecular crystals, such as structural transitions, metallizations, and superconductivity.

Solid hydrogen (H_2) is a typical example of molecular crystals, which was predicted to be a room-temperature superconductivity under high pressure,[3, 4] even though its metallization is still controversial in static pressure experiments.[5, 6] As an alternative, hydrogen-rich molecules crystal such as group IV hydrides (SiH_4, GeH_4, SnH_4) are extensively explored since their metallization can happen at relatively lower pressures, and they present a high superconducting critical temperature.[7-11] Another example is iodine, in part as analogs to H_2, which undergoes pressure-induced metallization and has a monatomic phase with superconductivity at higher pressure range.[12-14] Furthermore, some iodide (such as molecular crystal BI_3 and SnI_4) also turn out to be experienced a structural phase transition, metallization, and superconductivity under pressure.[15-19] The important insight into superconductivity under pressure can be obtained either from conventional Eliashberg theory[20] or non-traditional approach due to the local electron-electron interactions which have been successfully applied to nanosystems and organic molecules.[21] It is inspiring that the separate condensation of electron charge and spin degrees provides a new route for

superconductivity.[22]

The BI_3 molecule is a planar equilateral triangle structure formed with the boron atom at the center and three iodine atoms at the corners. At ambient condition, the molecule crystallizes into a hexagonal structure ($P6_3/m$ symmetry),[23] which is layered with the molecules lying in the planes perpendicular to *c* axis, as shown in Fig. 1. They are weakly bonded to those in the adjacent layers by van der Waals forces. On the other hand, the interaction inside one molecular plane is more complicated, which are intramolecular covalent and intermolecular halogen···halogen (I···I) interaction. Figure 1 shows the molecular structure of BI_3 and its electrostatic potential on the molecular surface (where red indicates negative, blue indicates positive). The positive region around the iodine atom cap would approach the negative "bay" between two iodine atoms of the neighboring molecules. Each iodine atom of BI_3 molecule contains positive cap and negative rim, and thus halogen···halogen is the key interaction in its crystal.

High-pressure phase transition and electronic properties of BI_3 have been investigated experimentally. A Raman spectra study showed that there was no obvious phase transition up to 5 GPa.[24] Later, X-ray diffraction experiment revealed a structural phase transition at 6.2 GPa to new phase with the face-centered-cubic lattice of iodine atoms.[15]. The resistivity measurements showed that the new phase become metallic at 23 GPa and exhibited superconductivity above 27 GPa.[15-17] The pressure dependence of T_c was positive changing from 0.5 to 1.9 K between 27 and 65 GPa. Since the atomic X-ray scattering power of boron is less than that of iodine, the boron atoms were not detected. In a recent theoretical study, Yao *et al.* calculated high pressure structure of BI_3 with *P*-1 symmetry by performed metadynamics algorithm and constructed fcc supercells that I atoms occupy fcc lattice and B atoms occupy interstitial sites.[25]

In the present work, we have searched for high-pressure structures of BI_3 by means of *ab initio*

evolutionary algorithm USPEX (Universal structure predictor: Evolutionary Xtallography).[26, 27] This method employed here are designed requiring only chemical compositions for a given compound to search for stable or metastable structures at given P/T conditions, which has been in correctly predicting high-pressure structures for various systems.[28, 29] It is found that planar molecular crystal of BI_3 transforms to dimer form with space group $P2_1/c$, and its superconductivity is mainly attributed to iodine vibrations. Our present study is an attempt to provide a better understanding of the nature of the structural and superconductivity properties of BI_3 crystal under high pressure.

Computational details

Evolutionary structure prediction was performed using the USPEX code, in conjunction with *ab initio* structure relaxations using density functional theory (DFT), as implemented in the Vienna *ab initio* simulation package VASP code.[30] The generalized gradient approximation (GGA) with the Perdew–Burke–Ernzerhof functional[31] was employed, because the GGA provides a much better treatment of planar molecular structure than the local density approximation.[32] The projector augmented wave (PAW) method [33] was adopted for B and I with electronic configuration of $2s^2 2p^1$ and $5s^2 5p^5$, respectively. The energy cutoff of 500 eV and appropriate Monkhorst-Pack *k* meshes were chosen to ensure that the total energy are well converged to better than 1 meV/atom. The lattice dynamics and electron-phonon coupling (EPC) calculations were carried out using linear response theory through the Quantum ESPRESSO package.[34] Convergence tests gave a kinetic energy cutoff of 50 Ry for $P2_1/c$ structure. The *q*-point mesh in the first BZ of 3×2×2 for $P2_1/c$ was adopted in the interpolation of the force constants for the phonon dispersion curve calculations. A denser 12×8×4 *k*-point mesh for $P2_1/c$ structure was used to ensure *k*-point sampling convergence with Gaussians of width 0.04 Ry, in order to approximate the zero-width limit in the calculations of the EPC parameter λ.

Results and discussion

We performed variable-cell structure prediction simulations using the above methodology for BI_3 with 2 f.u./cell at 1 GPa and 1-4 f.u./cell at pressure of 8 and 15 GPa, respectively. With the given information of chemical compositions on the crystal structure prediction, we were able to correctly reproduce the observed $P6_3/m$ structure (Fig. 1(a)) as the most stable structure at 1 GPa. Under high pressure, we got a series of promising candidate structures as shown in Fig. 2: two monoclinic $P2_1/c$ (4 f.u./cell), an orthorhombic $Imm2$ (2 f.u./cell), a monoclinic $C2/m$ (4 f.u./cell), and the lattice parameters and atomic positions of these structures at different pressure are listed in Table 1. The two $P2_1/c$ structure have the same B_2I_6 dimer that are isostructural with diborane molecule, but different in lattice parameters and the B_2I_6 dimer packing patterns. In one structure, B_2I_6 dimer forms zigzag sheets with $c/a>1$ (see in Fig. 2(a)), denoted as $P2_1/c$ ($c/a>1$), ,while for another structure, B_2I_6 dimer is characterized as parallel molecules configuration with $c/a<1$ (see in Fig. 2(b)), denoted as $P2_1/c$ ($c/a<1$). The $Imm2$ structure consists of infinite polymeric chains with alternating B and I atoms, as shown in Fig. 2(c), and the $C2/m$ structure is characterized as B_2I_6 dimer that are isostructural with ethane molecule, as shown in Fig. 2(d).

In order to identify the reasonability of the candidate structures, we compare the X-ray diffraction (XRD) patterns of these structures with the experimental pattern, as shown in Fig. 3. The experimental pattern of BI_3 (shown in Fig 3(a)) was obtained from Hamaya *et al.*'s work.[15] Theoretical ones are obtained by using the module of the Reflex in Materials Studio (MS) with the same X-ray wavelength of 0.32940 Å as the experimental one. We note that the XRD pattern of $P2_1/c$ ($c/a>1$) structure at 10 GPa is in an excellent agreement with the experimental pattern, as shown in Fig. 3. The main peaks of $P2_1/c$ ($c/a<1$) and $Imm2$ structures at $2\theta = 6.36°$ are consistent with the experimental data, however, there are many splitting for other

peaks. In the case of $C2/m$ structure, the XRD pattern deviates significantly from the experimental pattern.

The enthalpies of our suggested candidate structures relative to $P6_3/m$ structure are plotted in Fig. 4. It is shown that the enthalpy of $P2_1/c$ (c/a<1), $P2_1/c$ (c/a>1) and $Imm2$ is lower than that of $P6_3/m$ structure above the pressure of 3.1, 4.4 and 6.2 GPa, respectively. It is illustrated that the $P6_3/m$ structure become unstable between 3.1~6.2 GPa, which consistent with the experimentally observed above 6.2 GPa. The $P2_1/c$ (c/a<1) structure has the lowest enthalpy up to pressure of 11.7 GPa that the $C2/m$ structure occurs. However, the XRD patter of $C2/m$ structure is not consistent with the experimental data. Another $P2_1/c$ structure with c/a>1 has higher enthalpies than $P2_1/c$ (c/a<1) structure, but the XRD pattern of $P2_1/c$ (c/a>1) is more close to experimental data than that of $P2_1/c$ (c/a>1) structure. Moreover, it is noted that the enthalpy of $P2_1/c$ (c/a>1) is lower than that of previously proposed P-1 structure.[25] In addition, we compare the calculated equation of states for $P6_3/m$ and $P2_1/c$ together with the experimental data, as shown in Fig. 5. Excellent mutual agreement between theory and experiment gives another support for the validity of the $P2_1/c$ (c/a>1) structure. The volume collapses with 4.9% for $P6_3/m$ to $P2_1/c$ (c/a>1) transition suggesting the first-order phase transition character. Therefore, on the basis of a comparison of the total energies, X-ray diffraction patterns, and equation of states, we conclude that the structure of the high pressure phase closely resembles the $P2_1/c$ (c/a>1) structure. In order to more convenient writing, we denoted the $P2_1/c$ (c/a>1) structure as $P2_1/c$ in the following text.

To investigate the dynamical stability of $P2_1/c$, its phonon spectrum at different pressure has been calculated. The phonon band dispersion of the $P2_1/c$ structure can be seen in the left panel of Fig. 6, while the partial phonon density of states is shown in the right panel. The absence of imaginary frequency modes in the whole Brillouin zone in our study pressure range, indicates that this structure is dynamical stable. Two

separate regions of phonon bands are clearly recognized. As expected, the low frequencies are dominated by the vibrations of the iodine framework, whereas the high end of the spectrum is solely due to the light boron atoms.

To further understand the mechanical stability of the $P2_1/c$ structure, the elastic constants have been calculated. The mechanical stability of crystal requires the strain energy to be positive, which implies that all of the elastic constant C_{ij} satisfies Born stability criterion.[35] For the monoclinic phase crystal, the independent elastic stiffness tensor consists of thirteen components C_{11}, C_{22}, C_{33}, C_{44}, C_{55}, C_{66}, C_{12}, C_{13}, C_{15}, C_{23}, C_{25}, C_{35}, and C_{46} in the Voigt notation. The Born stability criteria for monoclinic system[36] are given by

$$
\begin{aligned}
&C_{ii} > 0,\ (\mathrm{i}=1,\ldots 6)\\
&[\mathrm{C}_{11} + C_{22} + C_{33} + 2(C_{12} + C_{13} + C_{23})] > 0,\\
&(C_{33}C_{55} - C_{35}^2) > 0,\ (C_{44}C_{66} - C_{46}^2) > 0,\\
&(C_{22} + C_{33} - 2C_{23}) > 0,\\
&[\mathrm{C}_{22}(C_{33}C_{55} - C_{35}^2) + 2C_{23}C_{25}C_{35} - C_{23}^2C_{55} - C_{25}^2C_{33})] > 0,\\
&\{2[\mathrm{C}_{15}\mathrm{C}_{25}(\mathrm{C}_{33}\mathrm{C}_{12} - \mathrm{C}_{13}\mathrm{C}_{23}) + \mathrm{C}_{15}\mathrm{C}_{35}(\mathrm{C}_{22}\mathrm{C}_{13} - \mathrm{C}_{12}\mathrm{C}_{23}) + \mathrm{C}_{25}\mathrm{C}_{35}(\mathrm{C}_{11}\mathrm{C}_{23} - \mathrm{C}_{12}\mathrm{C}_{13})]\\
&-[C_{15}^2(C_{22}C_{33} - C_{23}^2) + C_{25}^2(C_{11}C_{33} - C_{13}^2) + C_{35}^2(C_{11}C_{22} - C_{12}^2)] + C_{55}g\} > 0,\\
&(g = C_{11}C_{22}C_{33} - C_{11}C_{23}^2 - C_{22}C_{13}^2 - C_{33}C_{12}^2 + 2C_{12}C_{13}C_{23}).
\end{aligned}
$$

The elastic constants of the $P2_1/c$ structure calculated at different pressures are listed in Table 2. All of the elastic constants satisfy the Born stability criteria, suggesting that this structure is mechanical stable in our study pressure range.

With the knowledge of this halogen···halogen interaction model, we propose the following mechanism for the pressure-induced phase transition. At ambient pressure, the main intermolecular interaction is halogen···halogen (I···I) interaction within layers and van der Waals forces in the adjacent layers. In the low-pressure range, the application of pressure results mainly in the reduction of interlayer distance and the

increase of van der Waals interactions. The I···I interactions within each layer are also strengthened, but the interlayer distance reduces more than the distance between the molecules in the layers. On further compression, the layered structure gradually becomes unstable. At sufficient pressure, the covalent bond can no longer support the decreased volume and the increased energy of I···I networks interactions. Thus, the boron atoms are pushed out of the molecular plane and form a triangular pyramid molecular. The electrostatic potential on the triangular pyramid molecular surface are presented in Fig. 7(b). It is fascinating that the boron atom display positive, while one of the iodine atoms show stronger negative rim. Owing to these electrostatic interactions in the energetically favored position, each atom favors one short contact involving its positive region and one contact involving its negative region. Therefore, the boron atom closely contacts with the iodine atom of another BI_3 molecule, forming B_2I_6 dimer.

The calculated electronic band structure and projected density of states (PDOS) for boron and iodine of $P6_3/m$ and $P2_1/c$ at different pressures are shown in Fig. 8. At the ambient pressure, the $P6_3/m$ structure is an insulator with indirect band gap of 2.88 eV. Energy band structures are flat indicating that the $P6_3/m$ structure is a typical molecular crystal. With the increase of pressure, the energy bands become more dispersive and hybridization increases. When the pressure is increased above 30 GPa, the bands of the $P2_1/c$ structure starts to overlap as shown in Fig. 8(b), signals the onset of metallization. The metallization was mainly caused by I-derived valence band and I, B-derived conducting band which first cross the Fermi level.

The superconducting critical temperature can be estimated from the Allen-Dynes modified McMillan equation[20] $T_c = \frac{\omega_{log}}{1.2}\exp[-\frac{1.04(1+\lambda)}{\lambda-\mu^*(1+0.62\lambda)}]$, where λ is the electron-phonon coupling parameter, $\omega_{\log}$ is the logarithmic average frequency, and μ^* is the Coulomb pseudopotential. This equation has been found to

be highly accurate for materials with λ< 1.5. Because of the lack of knowledge of an appropriate value for the Coulomb potential μ^*, there is a great difficulty in accurate prediction of T_c. For the weak coupling materials, an empirical value of 0.1 for μ^* is often adopted. However, the value of μ^* in some materials are quite complex.[37-39] In view of the difficulties in determination of Coulomb pseudopotential, the T_c of $P2_1/c$ structure at several pressures have been calculated with four different values of μ* from 0.04 to 0.10. These results are summarized in Table 3. At a μ^* of 0.04, the superconducting critical temperature T_c is 0.24 K at 35 GPa, and increase to 1.9 K at 60 GPa, agrees well with the experimental value of 1.9 K at 65 GPa.[15] No matter what value of μ^*, the transition temperature of the $P2_1/c$ structure has the tendency to increase monotonically with applied pressure, which coincides with the experimental results.[15]

To probe the origin of superconducting properties in $P2_1/c$ structure, we calculated the EPC parameter λ, the logarithmic average phonon frequency ω_{log}, electronic density of states at the Fermi level $N(\varepsilon_f)$, and the Eliashberg phonon spectral function $\alpha^2F(\omega)$. The resulting λ is 0.372 at 60 GPa, indicating that the EPC is fairly weak, and the phonon frequency logarithmic average ω_{log} calculated directly from the phonon spectrum is 190 K, as listed in Table 3. The theoretical spectral function $\alpha^2F(\omega)$ and the integrated λ as a function of frequency at 60 GPa are predicted in Fig. 9. In conjunction with partial phonon density of states (see in Fig. 6), it is found that the contribution from the low frequency iodine translational vibrations constitutes 88.7% of the total λ. The high frequency derived from the boron vibrational mode make up a section of 11.3%. This result highlights the significant role played by iodine atoms on the superconductivity.

To study the pressure dependence of the superconducting critical temperature, values of λ, ω_{log}, and $N(\varepsilon_f)$ computed at selected pressures are summarized in Table 3. Assuming μ^* is a constant, two parameters,

EPC parameter λ and the logarithmic average frequency ω_{log} determine T_c. From the Table 3, we note that as the pressure increases, both λ and ω_{log} increase, which lead to the positive pressure dependence of T_c. Furthermore, EPC parameter λ of $P2_1/c$ structure is strongly linked to its electronic structure. It is shown that the electronic density of states at the Fermi level $N(\varepsilon_f)$ enhanced with increasing pressure. Therefore, the increase of T_c with pressure is due to the increase of λ, ω_{log}, and $N(\varepsilon_f)$, as listed in Table 3.

Conclusions

In summary, we explored the high pressure crystal structure and superconductivity properties of boron triiodide by means of *ab initio* calculations. We obtain the crystal structure of high pressure phase, which is a dimer molecular crystal with space group $P2_1/c$. Using this structure, the XRD, EOS, metallization pressure, and the positive pressure dependence of T_c are consistent with experimental results. Moreover, we propose a pressure-induced phase transition mechanism with halogen···halogen interaction model. Further electron-phonon coupling calculations show that the iodine vibration plays the major role in the superconductivity of BI_3, while the contribution from boron vibration is minor. In addition, the superconducting critical temperature T_c increases with increasing pressure mainly due to the increase of λ, ω_{log}, and $N(\varepsilon_f)$. This paper is helpful for achieving more insight into structure and superconductivity of BX_3 (X=Cl, Br) systems at high pressure.

Acknowledgements

This work was supported by the National Basic Research Program of China (No. 2011CB808200), Program for Changjiang Scholars and Innovative Research Team in University (No. IRT1132), National Natural Science Foundation of China (Nos. 51032001, 11074090, 11204100, 10979001, 51025206, 11104102), National Found for Fostering Talents of basic Science (No. J1103202), China Postdoctoral Science Foundation (2012M511326, 2013T60314), and Specialized Research Fund for the Doctoral Program of Higher Education (20120061120008, 20110061120007). Parts of calculations were performed in the High Performance Computing Center (HPCC) of Jilin University.

References

1. R. J. Hemley, *Annu. Rev. Phys. Chem.* , 2000, **51**, 763-800.
2. D. Li, K. Bao, F. Tian, X. Jin, D. Duan, Z. He, B. Liu and T. Cui, *RSC Adv.*, 2014, **4**, 203-207.
3. E. Wigner and H. B. Huntington, *J. Chem. Phys.*, 1935, **3**, 764-770.
4. N. W. Ashcroft, *Phys. Rev. Lett.*, 1968, **21**, 1748.
5. M. I. Eremets and I. A. Troyan, *Nat. Mater.*, 2011, **10**, 927-931.
6. C.-S. Zha, Z. Liu and R. J. Hemley, *Phys. Rev. Lett.*, 2012, **108**, 146402.
7. M. I. Eremets, I. A. Trojan, S. A. Medvedev, J. S. Tse and Y. Yao, *Science*, 2008, **319**, 1506-1509.
8. M. Martinez-Canales, A. R. Oganov, Y. Ma, Y. Yan, A. O. Lyakhov and A. Bergara, *Phys. Rev. Lett.*, 2009, **102**, 087005-087004.
9. G. Gao, A. R. Oganov, A. Bergara, M. Martinez-Canales, T. Cui, T. Iitaka, Y. Ma and G. Zou, *Phys. Rev. Lett.*, 2008, **101**, 107002-107004.
10. J. S. Tse, Y. Yao and K. Tanaka, *Phys. Rev. Lett.*, 2007, **98**, 117004-117004.
11. G. Gao, A. R. Oganov, P. Li, Z. Li, H. Wang, T. Cui, Y. Ma, A. Bergara, A. O. Lyakhov, T. Iitaka and G. Zou, *Proc. Natl Acad. Sci. USA*, 2010, **107**, 1317.
12. K. Takemura, S. Minomura, O. Shimomura and Y. Fujii, *Phys. Rev. Lett.*, 1980, **45**, 1881.
13. K. Shimizu, N. Tamitani, N. Takeshita, M. Ishizuka, K. Amaya and S. Endo, *J. Phys. Soc. Jpn.*, 1992, **61**, 3853-3855.
14. D. Duan, X. Jin, Y. Ma, T. Cui, B. Liu and G. Zou, *Phys. Rev. B*, 2009, **79**, 064518-064517.
15. N. Hamaya, M. Ishizuka, S. Onoda, J. Guishan, A. Ohmura and K. Shimizu, *Phys. Rev. B*, 2010, **82**, 094506.
16. S. Onoda and K. Shimizu, *J. Phys.: Conference Series*, 2008, **121**, 032008.
17. S. Onoda and K. Shimizu, *J. Phys. Soc. Jpn.* , 2007, **76**, 33.
18. N. Hamaya, K. Sato, K. Usui-Watanabe, K. Fuchizaki, Y. Fujii and Y. Ohishi, *Phys. Rev. Lett.*, 1997, **79**, 4597.
19. A. Ohmura, K. Sato, N. Hamaya, M. Isshiki and Y. Ohishi, *Phys. Rev. B*, 2009, **80**, 054201-054207.
20. P. B. Allen and R. C. Dynes, *Phys. Rev. B*, 1975, **12**, 905.
21. G. W. Fernando, A. N. Kocharian, K. Palandage, T. Wang and J. W. Davenport, *Phys. Rev. B*, 2007, **75**, 085109.
22. A. N. Kocharian, G. W. Fernando, K. Palandage and J. W. Davenport, *Phys. Rev. B*, 2008, **78**, 075431.
23. B. Albert and K. Schmitt, *Z. Anorg. Allg. Chem.* , 2001, **627**, 809-810.
24. A. Anderson and L. Lettress, *J. Raman Spectrosc.*, 2002, **33**, 173-176.
25. Y. Yao, D. D. Klug, Martoncaron, aacute, R. k and S. Patchkovskii, *Phys. Rev. B*, 2011, **83**, 214105.
26. A. R. Oganov and C. W. Glass, *J. Chem. Phys.*, 2006, **124**, 244704-244715.
27. A. R. Oganov, A. O. Lyakhov and M. Valle, *Acc. Chem. Res.* , 2011, **44**, 227-237.
28. A. R. Oganov, J. Chen, C. Gatti, Y. Ma, Y. Ma, C. W. Glass, Z. Liu, T. Yu, O. O. Kurakevych and V. L. Solozhenko, *Nature*, 2009, **457**, 863-867.
29. Y. Ma, M. Eremets, A. R. Oganov, Y. Xie, I. Trojan, S. Medvedev, A. O. Lyakhov, M. Valle and V. Prakapenka, *Nature*, 2009, **458**, 182-185.
30. G. Kresse and J. Furthmüller, *Phys. Rev. B*, 1996, **54**, 11169-11186.
31. K. B. John P. Perdew, *Int. J. Quantum Chem.*, 1996, **57**, 309-319.

32. D. Duan, Y. Liu, Y. Ma, Z. Liu, T. Cui, B. Liu and G. Zou, *Phys. Rev. B*, 2007, **76**, 104113-104118.
33. G. Kresse and D. Joubert, *Phys. Rev. B*, 1999, **59**, 1758-1775.
34. P. Giannozzi, S. Baroni, N. Bonini, M. Calandra, R. Car, C. Cavazzoni, D. Ceresoli, G. L. Chiarotti, M. Cococcioni, I. Dabo, A. D. Corso, S. d. Gironcoli, S. Fabris, G. Fratesi, R. Gebauer, U. Gerstmann, C. Gougoussis, A. Kokalj, M. Lazzeri, L. Martin-Samos, N. Marzari, F. Mauri, R. Mazzarello, S. Paolini, A. Pasquarello, L. Paulatto, C. Sbraccia, S. Scandolo, G. Sclauzero, A. P. Seitsonen, A. Smogunov, P. Umari and R. M. Wentzcovitch, *J. Phys.: Condens. Matter*, 2009, **21**, 395502.
35. M. B. a. K. Huang, *Dynamical Theory of Crystal Lattice*, Claren-don, Oxford, 1956.
36. Z. Wu, E. Zhao, H. Xiang, X. Hao, X. Liu and J. Meng, *Phys. Rev. B*, 2007, **76**, 054115-054115.
37. C. Richardson and N. Ashcroft, *Phys. Rev. B*, 1997, **55**, 15130.
38. Y. Ma, J. S. Tse, T. Cui, D. D. Klug, L. Zhang, Y. Xie, Y. Niu and G. Zou, *Phys. Rev. B*, 2005, **72**, 014306-014309.
39. Y. Yao and J. Tse, *Phys. Rev. B*, 2007, **75**, 134104.

Captions

Fig. 1 Top: planar sheets and calculated electrostatic potential on the molecular surface of BI_3. The electrostatic potential scale ranges from -0.0074 au (red) to 0.0074 au (blue). Bottom: crystal structure of BI_3 at ambient pressure. The small gray balls denote the boron atoms, and the big blue ones denote iodine atoms.

Fig. 2 The crystal structure of (a) $P2_1/c$ with $c/a>1$, (b) $P2_1/c$ with $c/a<1$, (c)$Imm2$, and (d) $C2/m$.

Fig. 3 Comparison of the experimental X-ray powder diffraction pattern of high pressure phase at 9.1 GPa with that of our calculated structures at selected pressure.

Fig. 4 The enthalpies per BI_3 unit of our calculated structures as functions of pressure with respect to the enthalpies of $P6_3/m$ structure.

Fig. 5 Calculated equation of states (EOS) of BI_3 is compared with experimental data. Our calculated results of $P6_3/m$ and $P2_1/c$ ($c/a>1$) structures are denoted by solid olive triangles and pink squares, respectively. The experimental data are denoted by open circles (ref. 15).

Fig. 6 The calculated phonon band structures and projected PHDOS for $P2_1/c$ structure at different pressures.

Fig. 7 The schematic diagram of BI_3 molecular dimerization. (a) planar BI_3 molecular of $P6_3/m$ structure, (b) electrostatic potential on the triangular pyramid molecular surface, (c) dimer B_2I_6 molecular of phase $P2_1/c$ structure.

Fig. 8 The calculated electronic band structure and DOS projected on B and I atoms for $P6_3/m$ and $P2_1/c$ structures at 0 and 30 GPa, respectively.

Fig. 9 The calculate Eliashberg phonon spectral function $\alpha^2F(\omega)$ and the electron-phonon integral $\lambda(\omega)$ of $P2_1/c$ at 60 GPa.

Table 1 Structure parameters of our predicted $P2_1/c$ ($c/a>1$), $P2_1/c$ ($c/a<1$), $Imm2$ and $C2/m$ for BI_3 at selected pressure.

Table 2 The calculated elastic constants (in GPa) of $P2_1/c$ structure at different pressures.

Table 3 The electron-phonon coupling parameter λ, electronic density of states at the Fermi level $N(\varepsilon_f)$ (states/spin/Ry/unit cell), logarithmic average of vibrational frequencies ω_{log}, and superconducting critical temperature T_c computed in $P2_1/c$ structure at different pressures.

Figures

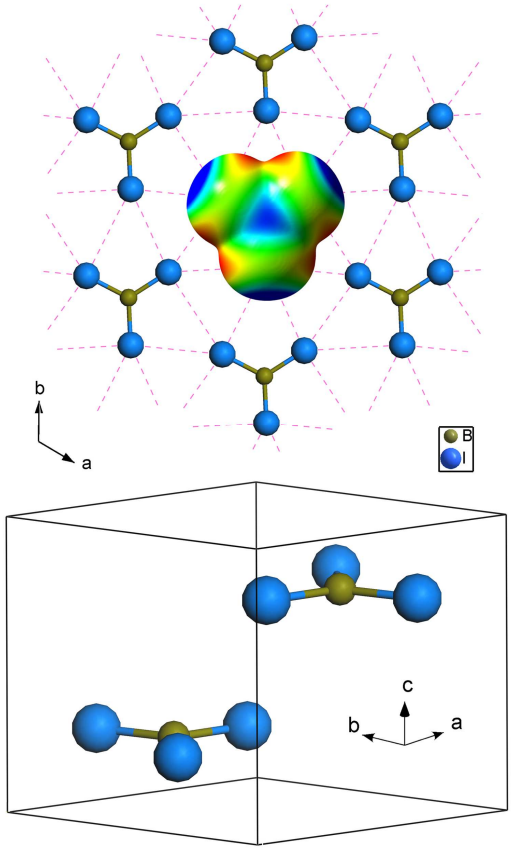

Fig. 1

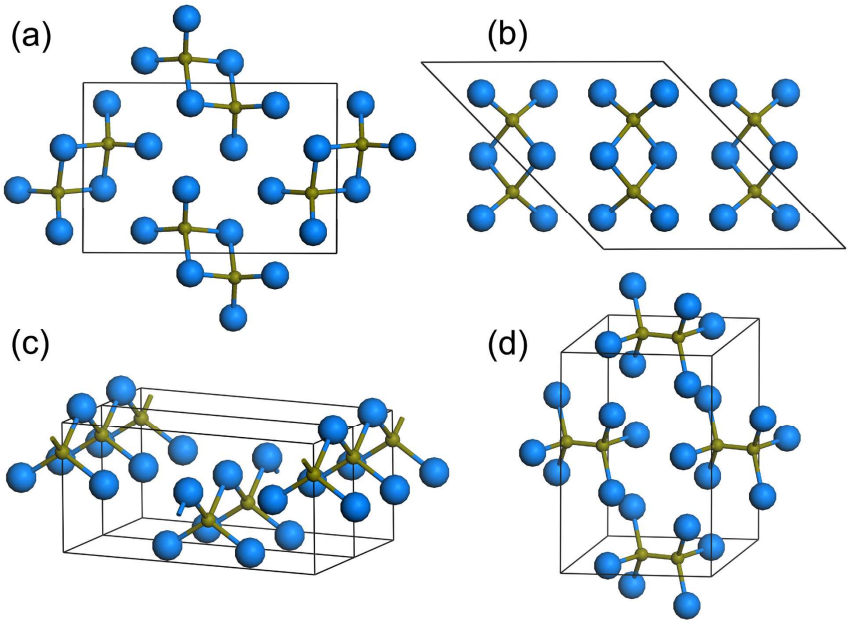

Fig. 2

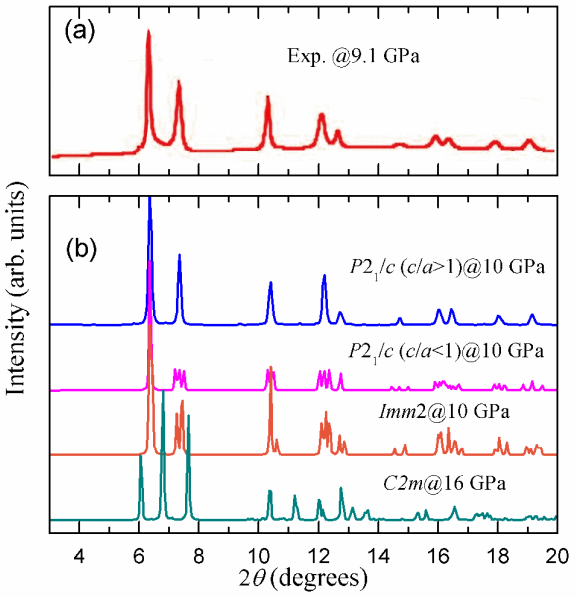

Fig. 3

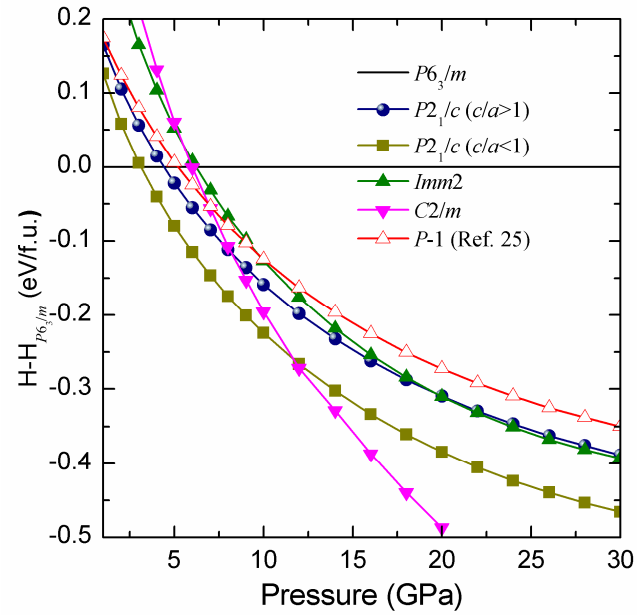

Fig. 4

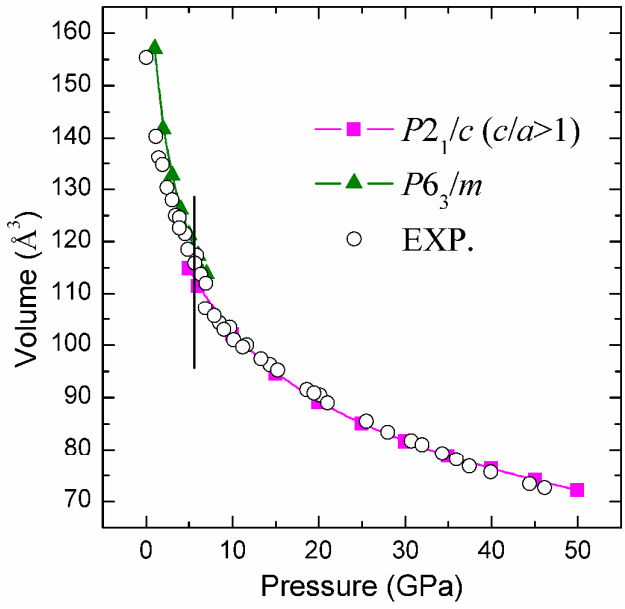

Fig. 5

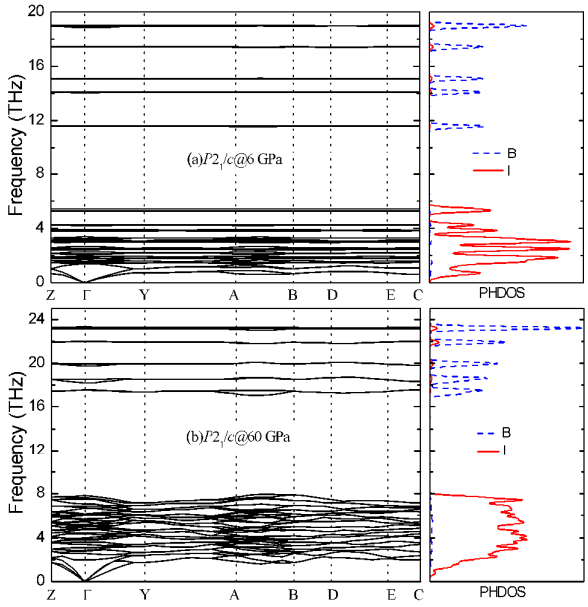

Fig. 6

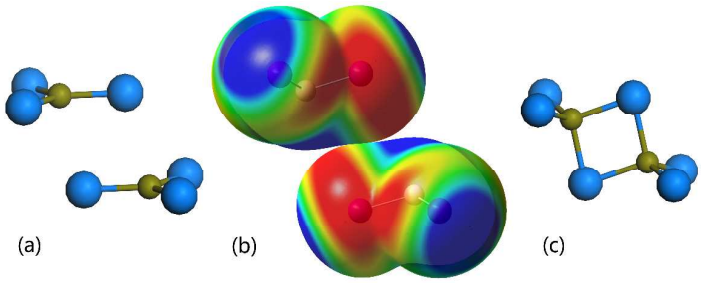

Fig. 7

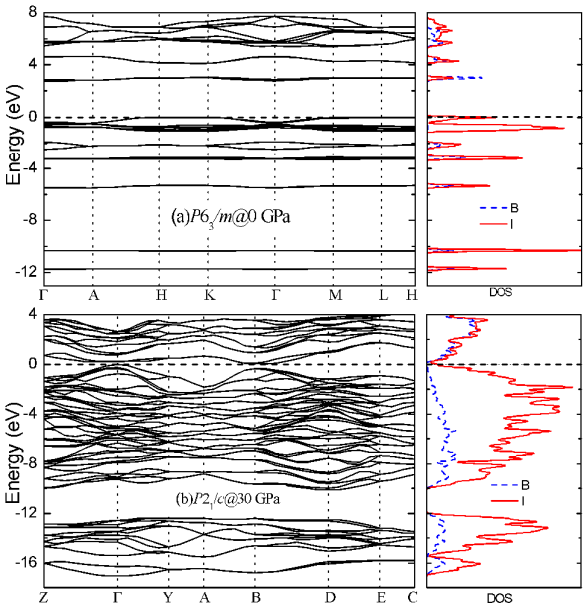

Fig. 8

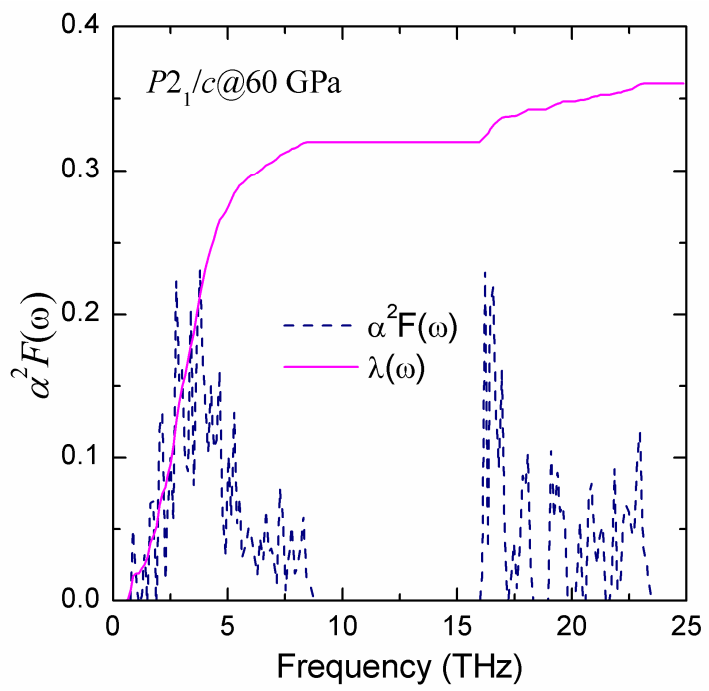

Fig. 9

Tables

Table 1

Space group	Lattice parameters (Å, °)	Atom	Atomic coordinates (fractional)		
			x	*y*	*z*
$P2_1/c$	*a*=5.15	B(4e)	-0.0980	0.1431	0.4013
c/*a*>1	*b*=7.31	I(4e)	-0.3476	0.3765	0.4074
(10 GPa)	*c*=12.06	I(4e)	-0.0161	0.1298	0.2425
	β=115.51	I(4e)	0.3106	0.1190	0.5769
$P2_1/c$	*a*=14.84	B(4e)	0.3094	-0.5010	0.7622
c/*a*<1	*b*=5.15	I(4e)	0.8330	-0.7502	1.5438
(10 GPa)	*c*=10.09	I(4e)	0.5005	0.2301	0.3800
	β=148.04	I(4e)	0.1689	0.2524	0.2163
Imm2	*a*=10.90	B(2a)	0.5	0.5	0.2666
(10 GPa)	*b*=3.56	I(4c)	0.3354	0.5	0.0442
	c=5.20	I(2b)	0.5	0	0.5446
*C*2/*m*	*a*=6.54	B(4i)	0.1316	0.5	0.5381
(16 GPa)	*b*=10.02	I(8j)	0.2393	0.1761	0.2510
	c=5.81	I(4i)	-0.2582	0.5	0.7714
	β=106.77				

Table 2

	6 GPa	15 GPa	30 GPa	60 GPa
C_{11}	53.481	117.269	194.261	330.469
C_{22}	59.190	133.276	221.742	318.474
C_{33}	77.613	160.565	267.566	438.777
C_{44}	16.055	29.734	45.799	39.176
C_{55}	15.993	34.407	56.256	82.709
C_{66}	24.517	50.439	82.768	122.927
C_{12}	27.980	61.104	104.871	151.013
C_{13}	21.709	44.896	78.567	156.757
C_{15}	6.955	15.967	24.942	31.068
C_{23}	15.379	34.131	68.477	148.927
C_{25}	-3.032	-11.442	-20.041	-47.894
C_{35}	-1.262	-6.654	-20.041	-27.083
C_{46}	-2.937	-8.617	-14.061	-2.662

Table 3

P (GPa)	ω_{log} (K)	$N(\varepsilon_f)$	λ	T_c (K) μ^*=0.04	T_c (K) μ^*=0.06	T_c (K) μ^*=0.08	T_c (K) μ^*=0.10
35	166.234	15.249	0.250	0.236	0.105	0.036	0.009
50	187.123	19.660	0.314	0.925	0.558	0.302	0.140
60	190.012	21.908	0.372	1.908	1.325	0.862	0.515

Table of Contents

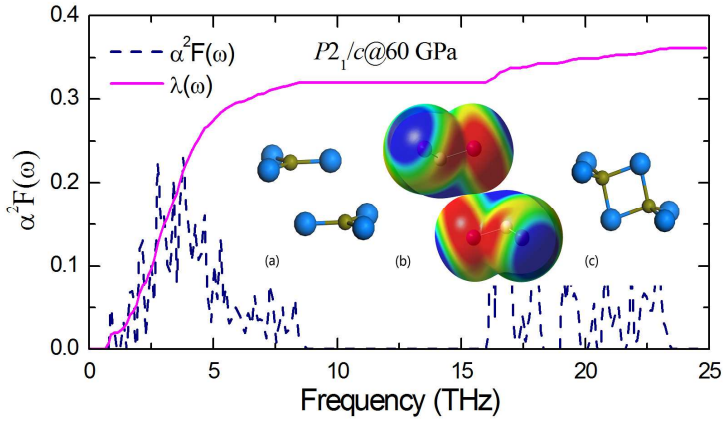

Planar BI_3 molecule transforms to dimer B_2I_6 ($P2_1/c$) under high pressure, and its superconductivity is mainly attributed to iodine vibrations.

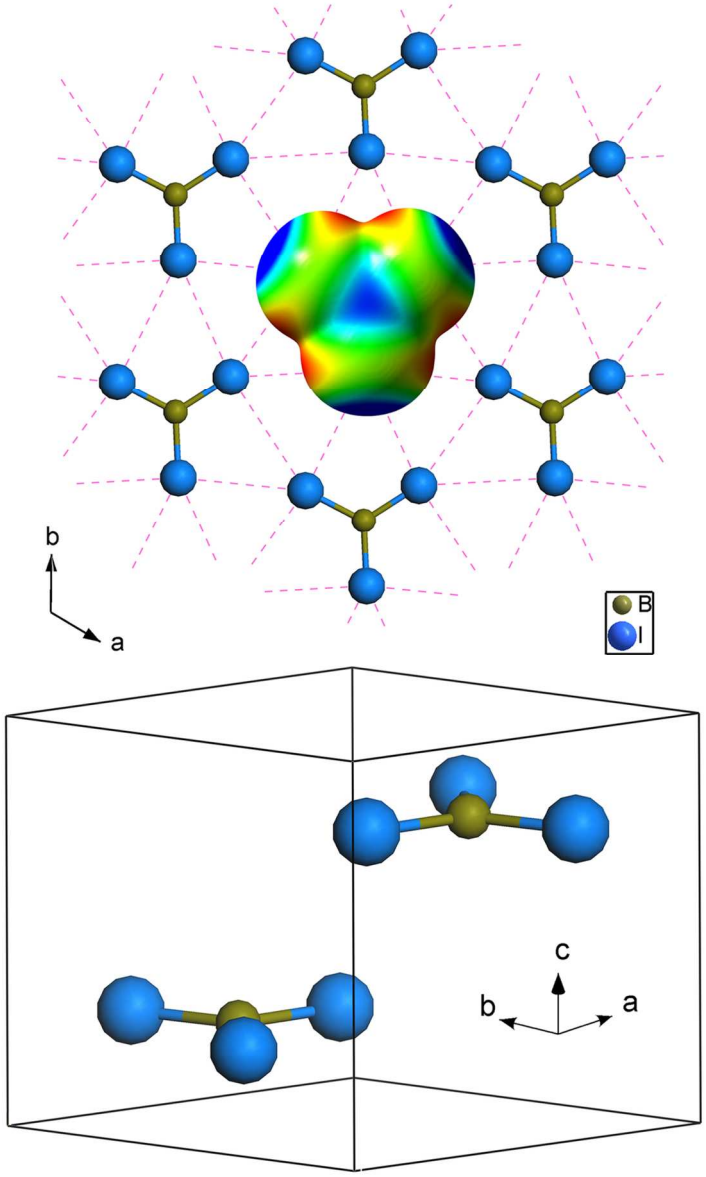

Fig. 1 Top: planar sheets and calculated electrostatic potential on the molecular surface of BI3. The electrostatic potential scale ranges from -0.0074 au (red) to 0.0074 au (blue). Bottom: crystal structure of BI3 at ambient pressure. The small gray balls denote the boron atoms, and the big blue ones denote iodine atoms.
98x160mm (300 x 300 DPI)

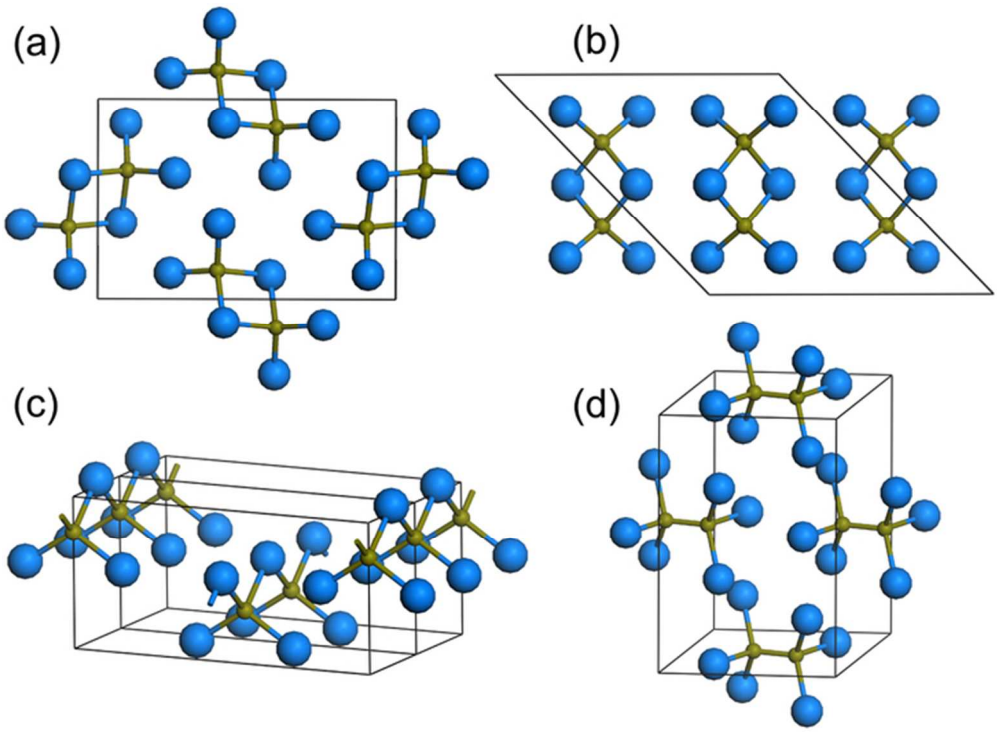

Fig. 2 The crystal structure of (a) P21/c with c/a>1, (b) P21/c with c/a<1, (c)Imm2, and (d) C2/m.
61x46mm (300 x 300 DPI)

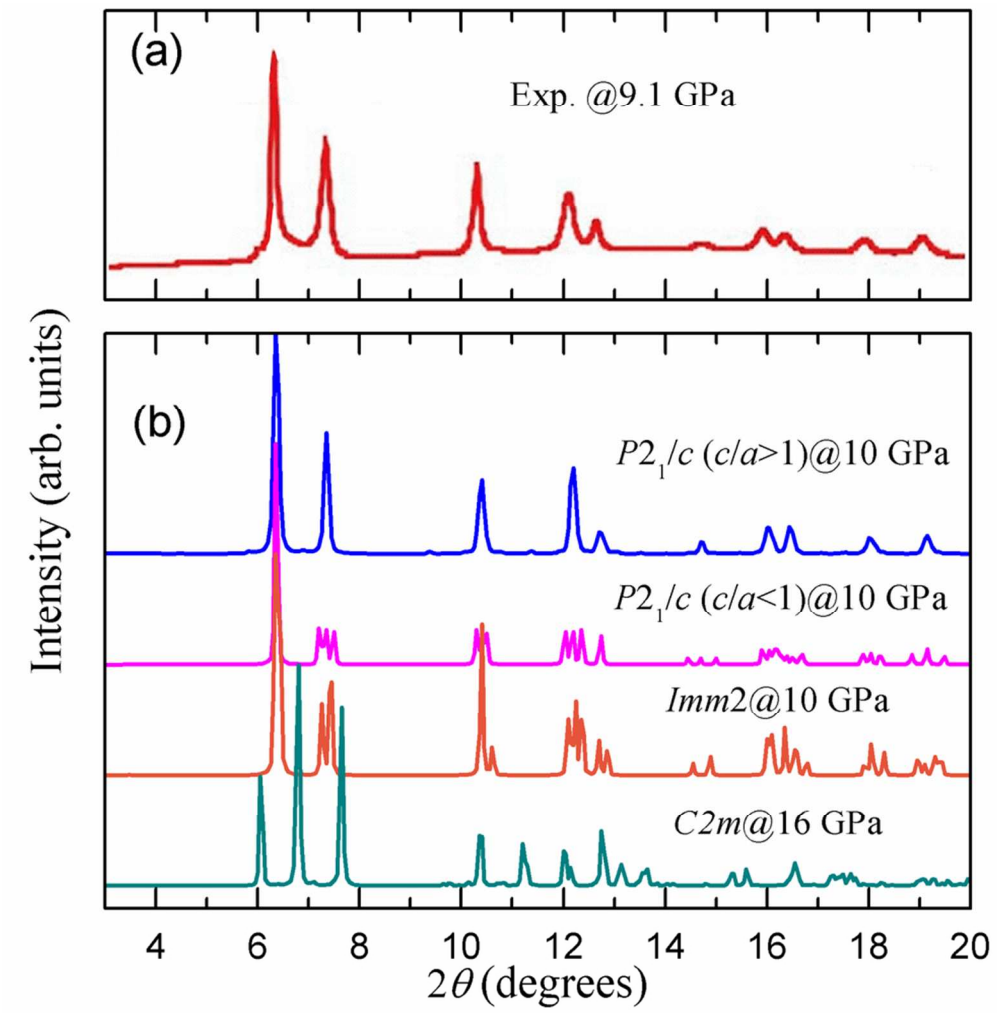

Fig. 3 Comparison of the experimental X-ray powder diffraction pattern of high pressure phase at 9.1 GPa with that of our calculated structures at selected pressure.
83x84mm (300 x 300 DPI)

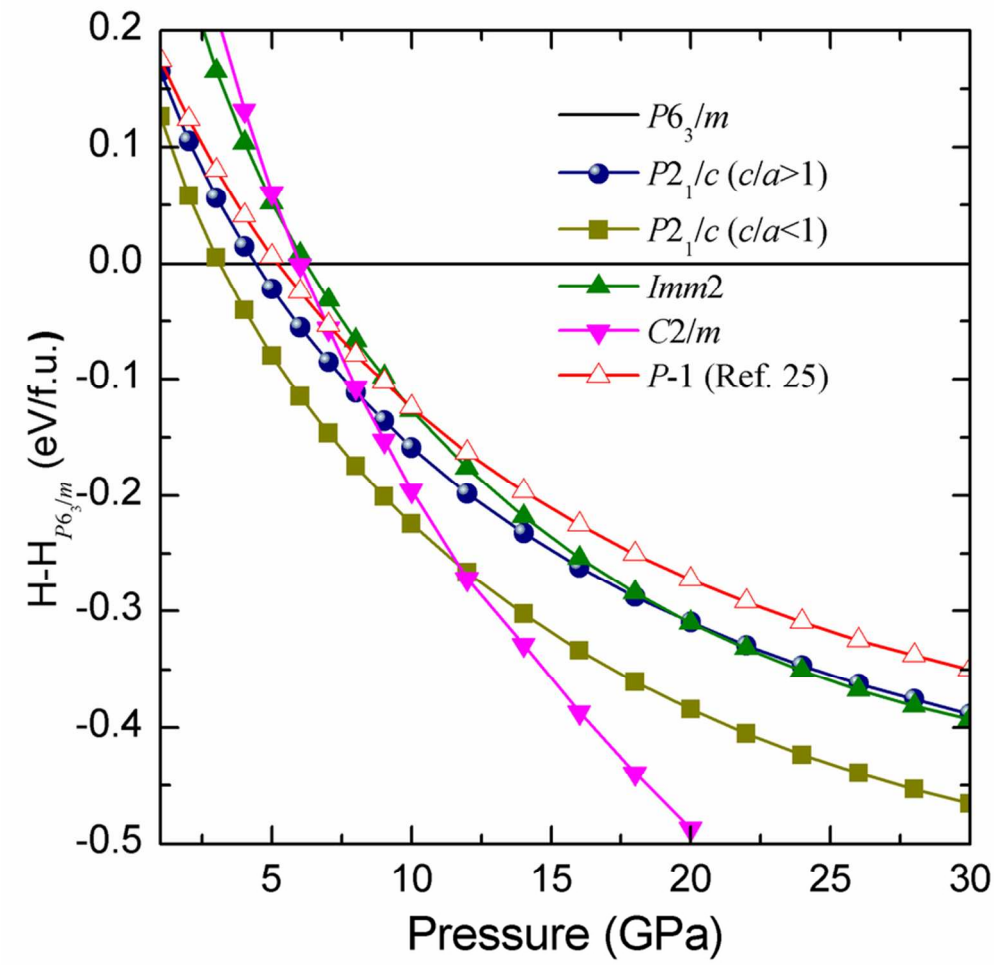

Fig. 4 The enthalpies per BI3 unit of our calculated structures as functions of pressure with respect to the enthalpies of P63/m structure.
80x77mm (300 x 300 DPI)

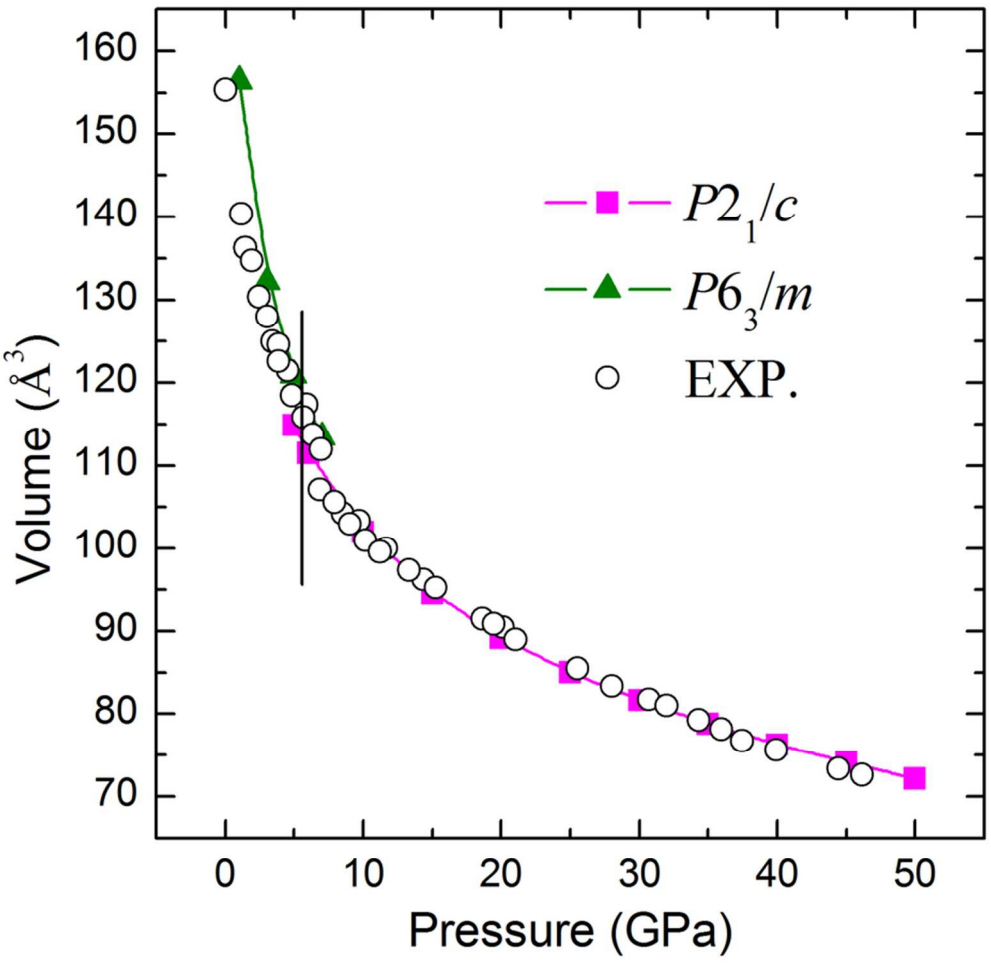

Fig. 5 Calculated equation of states (EOS) of BI3 is compared with experimental data. Our calculated results of P63/m and P21/c (c/a>1) structures are denoted by solid olive triangles and pink squares, respectively. The experimental data are denoted by open circles (ref. 15).
79x76mm (300 x 300 DPI)

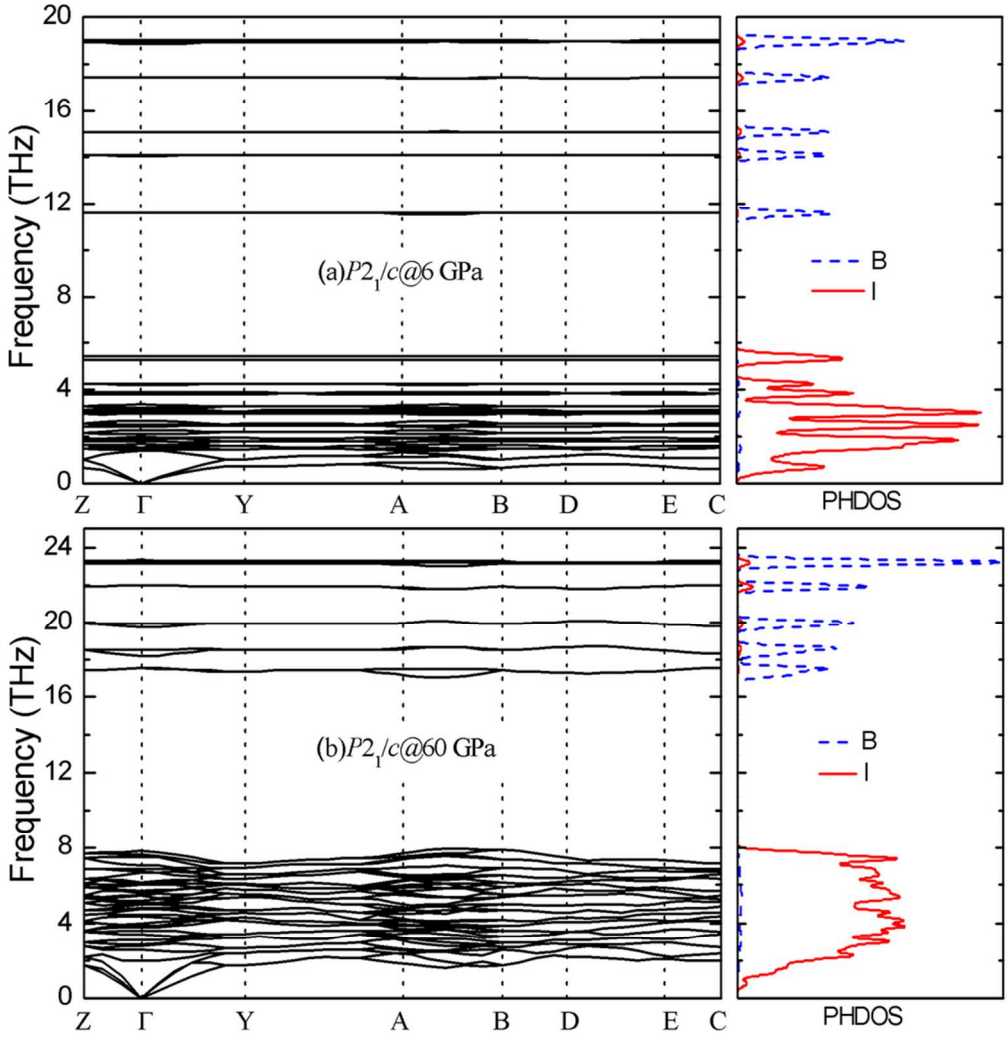

Fig. 6 The calculated phonon band structures and projected PHDOS for P21/c structure at different pressures.
84x88mm (300 x 300 DPI)

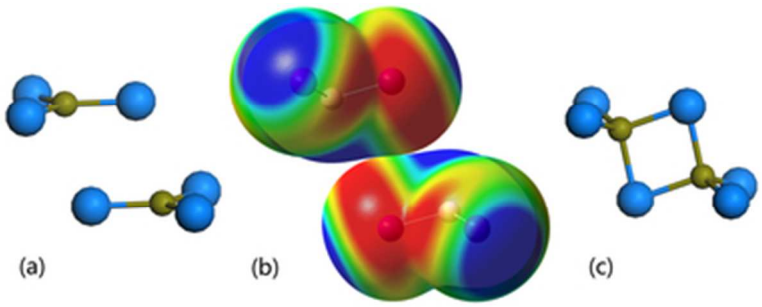

Fig. 7 The schematic diagram of BI3 molecular dimerization. (a) planar BI3 molecular of P63/m structure, (b) electrostatic potential on the triangular pyramid molecular surface, (c) dimer B2I6 molecular of phase P21/c structure.
32x12mm (300 x 300 DPI)

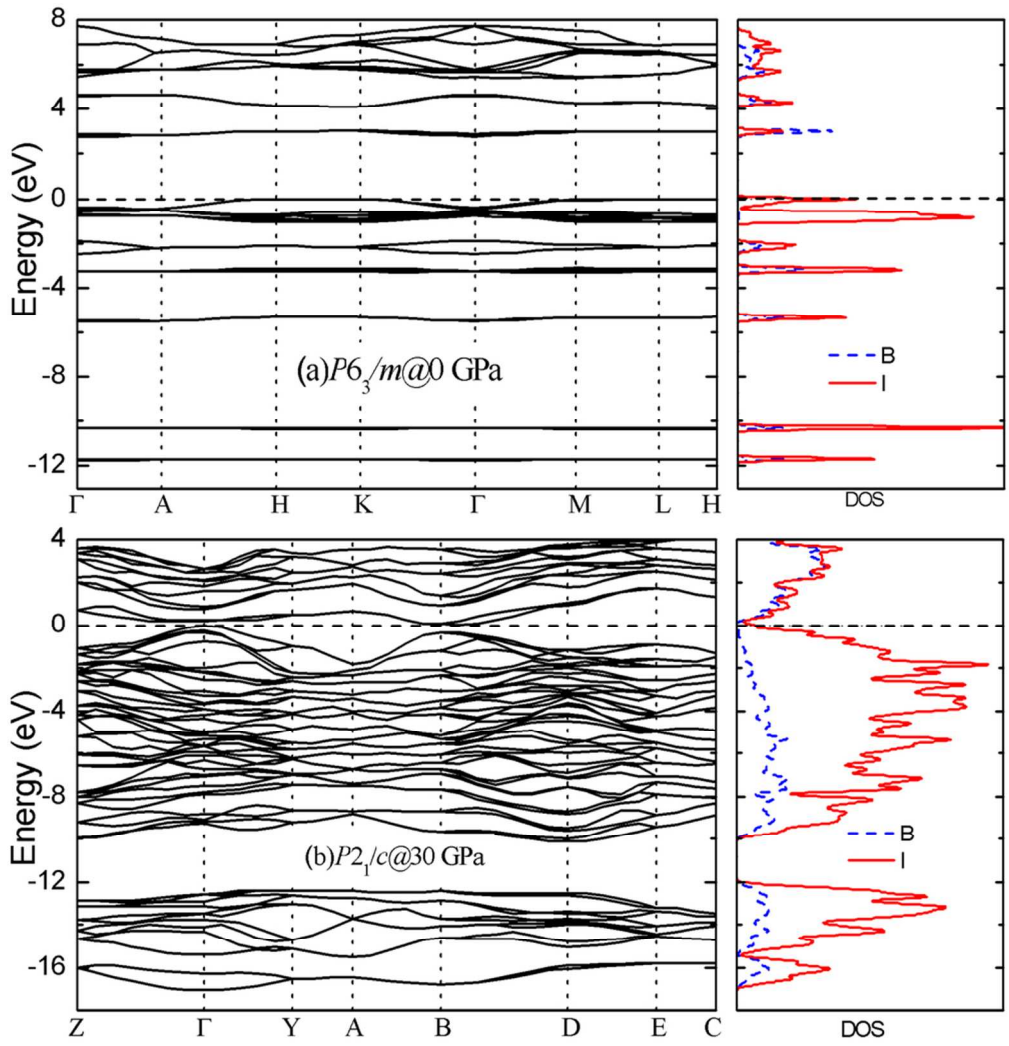

Fig. 8 The calculated electronic band structure and DOS projected on B and I atoms for P63/m and P21/c structures at 0 and 30 GPa, respectively.
84x87mm (300 x 300 DPI)

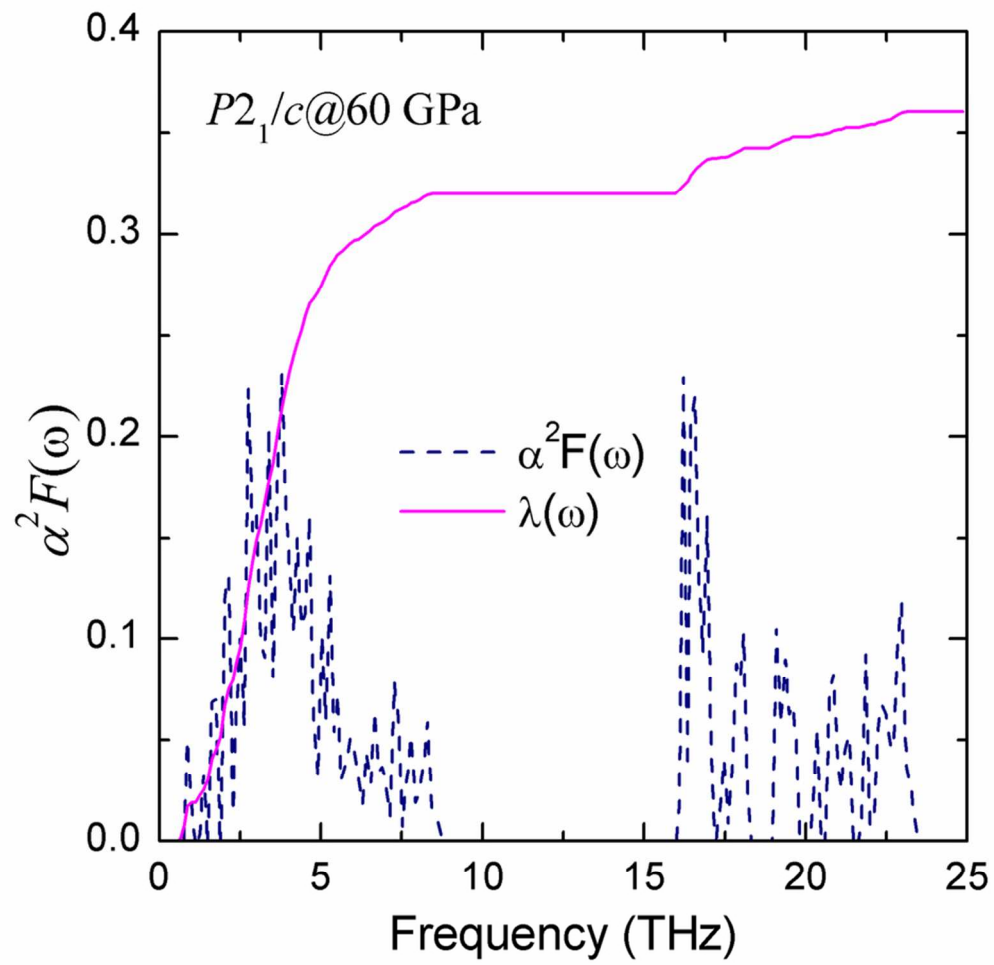

Fig. 9 The calculate Eliashberg phonon spectral function α2F(ω) and the electron-phonon integral λ(ω) of P21/c at 60 GPa.
80x77mm (300 x 300 DPI)

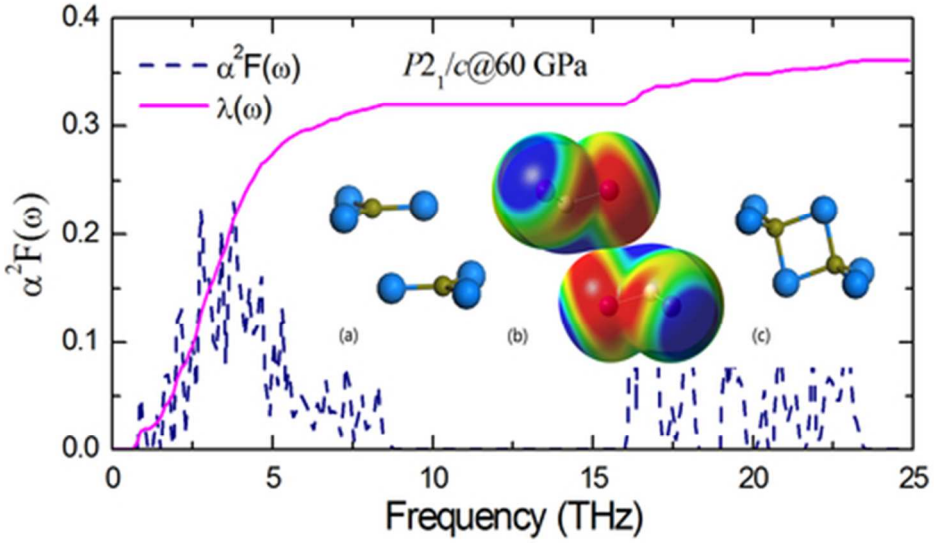

Table of Contents: Planar BI3 molecule transforms to dimer B2I6 (P21/c) under high pressure, and its superconductivity is mainly attributed to iodine vibrations.
39x23mm (300 x 300 DPI)